Bulletin of the Seismological Society of America, Vol. 102, No. 6, pp. 2667–2676, December 2012, doi: 10.1785/0120110349

Possible Earthquake Rupture Connections on Mapped California Faults Ranked by Calculated Coulomb Linking Stresses

by Tom Parsons, Edward H. Field, Morgan T. Page, and Kevin Milner

Abstract Probabilistic seismic hazard assessment is requiring an increasingly broad compilation of earthquake sources. Fault systems are often divided into characteristic ruptures based on geometric features such as bends or steps, though events such as the 2002 *M* 7.9 Denali, and 2011 *M* 9.0 Tohoku-Oki earthquakes raise the possibility that earthquakes can involve subsidiary faults and/or rupture through identified geometric barriers. Here we introduce a method to discriminate among a wide range of possible earthquakes within a large fault system and to quantify the probability of a rupture passing through a bend or step. We note that many of the conditions favoring earthquake rupture propagation can be simulated using a static Coulomb stress change approximation. Such an approach lacks inertial effects inherent in a full dynamic simulation but does capture many of the empirical observations drawn from examining past ruptures, such as continuity of rake and strike, as well as distance across gaps or stepovers. We make calculations for a test region in northern California and find that the method provides a quantitative basis for ranking possible ruptures within localized fault systems.

Introduction

Fault-based earthquake forecasts require decisions about the connectivity of the fault network. For example, can future ruptures propagate through sharp bends, branch off onto subsidiary faults, or jump across observed fault interruptions and/or stepovers? The critical offset distance for an earthquake to jump through a stepover is thought to be about 3–5 km, based on observations and numerical modeling (Barka and Kandinsky-Cade, 1988; Harris, 1992; Harris and Day, 1993, 1999; Kase and Kuge, 1998; Lettis *et al.*, 2002; Oglesby, 2008; Wesnousky, 2008; Elliott *et al.*, 2009; Lozos *et al.*, 2011). However, these investigators also point out that rupture continuity and branching is situational, depending on a variety of factors including: (1) whether the stepover is releasing or restraining, (2) the relative orientations and stress states on faults, (3) rake variations, and (4) slip distribution within the rupture. Therefore, the simple rule-of-thumb of fault separation distance is not a sufficient criterion for decision making.

Generally, fault-based earthquake forecasts rely on geological segmentation (e.g., McCann *et al.*, 1979; Working Group on California Earthquake Probabilities (WGCEP), 1988, 1990, 1995, 2003; Frankel *et al.*, 2002; Earthquake Research Committee, 2005; Romeo, 2005; Petersen *et al.*, 2008; Field *et al.*, 2009), which defines minimum/maximum rupture extents by identifying geometrical features of fault zones thought to arrest ruptures. This concept has observational basis from paleoseismology (e.g., Schwartz and Coppersmith, 1984; Wesnousky, 1994; Liu-Zeng *et al.*, 2007; Zielke *et al.*, 2010; Klinger *et al.*, 2011). However, as we observe more current large earthquakes in detail, we note surprising involvement of relatively minor (and sometimes previously unrecognized) faults in combination with major faults. For example, the 2002 *M* 7.9 Denali earthquake "began with thrusting on the previously unrecognized Susitna Glacier fault, continued with right-slip on the Denali fault, then took a right step and continued with right-slip on the Totschunda fault" (Eberhart-Phillips *et al.*, 2003). The 2008 *M* 8.0 Wenchuan earthquake occurred on three distinct and subparallel surface ruptures (Li *et al.*, 2008). Further, the 2011 *M* 9.0 Tohoku-Oki earthquake ruptured through defined segment boundaries and was unexpected (National Seismic Hazard Maps for Japan, 2005). The relative rates of these types of earthquakes are very difficult to forecast from a fault-based model, but recent experience shows that we clearly need to consider their possibility.

Computationally intensive methods exist to consider all possible ruptures within complex fault systems (e.g., Field and Page, 2011); however, geologically based decision making regarding branching and stepping ruptures on a case-by-case basis for thousands of fault combinations is impractical, if not impossible. Even if detailed geological information is available, it may be wise to augment it with mechanical modeling. This is the path intended for application by the Uniform California Earthquake Rupture Forecast (UCERF), wherein empirical rules built from observations of past

ruptures (e.g., Wesnousky, 2006; Klinger, 2010; Scholtz *et al.*, 2010; Wechsler *et al.*, 2010; Wesnousky and Biasi, 2011; Biasi *et al.*, 2012) are used in concert with mechanical modeling presented here.

If we want to create an earthquake rupture forecast that considers all possible fault combinations, we require a basis for ranking possible ruptures that is as sensitive as practical to specific geometries throughout a fault system and that can be consistently applied. While considering all possible ruptures, we seek a means to rank them from least to most viable. Ideally, fully dynamic earthquake simulations would be calculated for every rupture; however, at present, the computational and parameter demands of this exceed capability.

In this paper we introduce the concept of Coulomb linking stresses. This is an exploration into the use of static stress transmission as a proxy for dynamic rupture propagation. The static solution lacks the inertial components of a fully dynamic solution but can capture many of the other features thought to promote or inhibit rupture propagation from one fault section to another, including many that are commonly included in geological assessments. These include distance between sections, overlap, relative rakes, dips, and changes in strike. We therefore rank proposed earthquake ruptures by their links as a means of answering the question, does this particular earthquake rupture path through a junction, bend, step, or branch make more or less physical sense than another choice?

Method

An effective earthquake rupture forecast must specify as accurately as possible the complete magnitude distribution that will affect a region. This is generally accomplished with geological observations on fault geometry to identify likely rupture dimensions. Here we explore the idea that static stress transfer can capture and quantify the majority of these observations, while enabling consideration of massive numbers of possibilities. Coulomb stress change values are sensitive to distance, being much stronger with proximity. Thus the calculations may encompass rule-of-thumb ideas about fault steps and gaps derived from empirical studies. Further, Coulomb stress change magnitudes are larger when stress is transferred to compatible rakes. For example, stress changes are negative between along-strike right-lateral and left-lateral fault subsections, but would be positive between a strike-slip and orthogonal thrust fault link that are appropriately located to accommodate tectonic strain (Fig. 1). Thus static stress calculations can capture mechanically sensible fault junctions

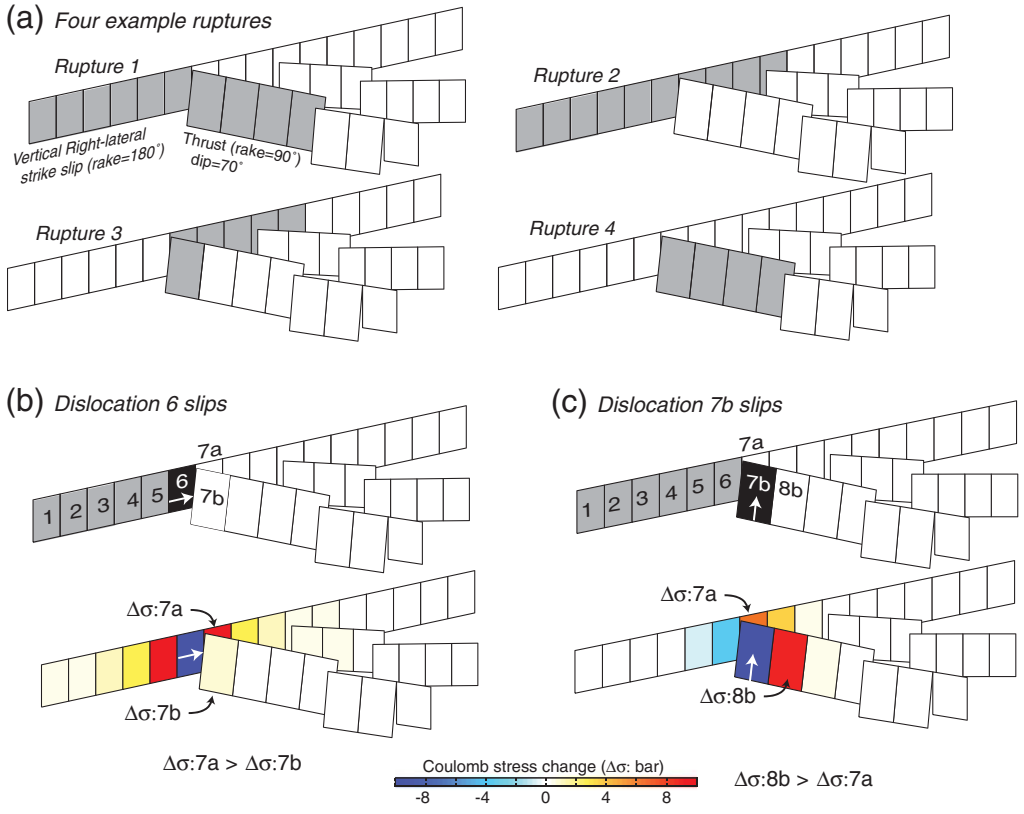

Figure 1. Example calculations. (a) Rectangles show the fault subsections within four potential ruptures that we use to assess the relative viability of each model. The ruptures in these examples can branch between vertical strike-slip faults and dipping thrusts. (b) Dislocation number 6, which lies at a fault junction, slips 0.1 m. It causes a larger static stress change on subsection 7a than on 7b, which would cause rupture 2 to be more favored than rupture 1 when all the linking stresses are averaged. (c) Dislocation number 7b is slipped, which increases stress at 8b more than at 7a, implying that rupture 4 is more favored than rupture 3, but only slightly. Slip at 7b puts dislocations 5 and 6 into a stress shadow, which implies that a potential rupture going the reverse direction on the strike-slip fault is not mechanically viable.

and penalize those that, while lying within the commonly invoked 3–5 km distance criterion, are not mechanically viable. Other examples that would be penalized are closely spaced, parallel subsections with the same rakes, because slip on one puts the other into a stress shadow.

Development of the UCERF includes cataloging all known active faults in California as seismic sources (e.g., Field *et al.*, 2009). These faults are broken into subsections that extend through the complete seismogenic thickness (typically 12–15 km) and are ~half the seismogenic thickness in length (Fig. 2). Each subsection has known or estimated dip and rake values assigned.

The UCERF goal is to consider all possible earthquake ruptures in California. A "possible" rupture means any combination of mapped fault subsections that does not have one of the following characteristics: (1) full-circle ruptures that start and stop at the same point, (2) U-turn ruptures that reverse direction by taking a greater than 90° turn, and (3) very long stepping ruptures that jump across distances in excess of 10 km. All other combinations are considered possible, though many may be very unlikely. The list of possible ruptures includes those that occur on a single defined fault as well as ones that branch onto other faults. The smallest ruptures in the model occupy two subsections; they then systematically include additional subsections up to the longest maximum extent as defined by the mapped fault system. Each fault branch or junction represents another series of possible ruptures, as every choice is explored out to maximum extent.

We begin with a list of adjacent subsections (<5 km apart) from within the California fault model. Subsection boundaries are defined arbitrarily along a fault (but are exactly adjacent on continuous faults) and constrained to end at geologically defined steps. Subsection boundaries thus do not have any unintended effect on stress change calculations. Fault geometry and rake data are used to create an elastic dislocation model for each subsection with the methods of Okada (1992) and Simpson and Reasenberg (1994). Our goal is to rank every junction in a relative way, so each source dislocation is assigned uniform slip of 0.1 m. Each subsection is broken down into 1 km by 1 km dislocations to preserve proper scaling and to accurately depict complex geometries. Static stress change is calculated by solving for Coulomb failure stress ($\Delta\sigma$) as $\Delta\sigma \equiv |\Delta\bar{\tau}_f| + \mu(\Delta\sigma_n - \Delta p)$, where $\Delta\bar{\tau}_f$ is the change in shear stress on the receiver fault (set positive in the rake direction), μ is the coefficient of friction, $\Delta\sigma_n$ is the change in normal stress acting on the target fault (set positive for unclamping), and Δp is pore pressure change (neglected here). Throughout the model, we used a constant slip of 0.1 m, a Coulomb stress calculated using a constant friction coefficient of $\mu = 0.5$, and shear stress calculated using friction coefficient of $\mu = 0.0$ because we are interested in direct comparison of different possible ruptures, and we want to treat them uniformly.

The geographic center is determined for each pair of subsections, and the dislocation models for that junction are projected into a local coordinate system using a Mercator projection in kilometers. Coulomb stress changes are systematically calculated using each dislocation within the pair of fault subsections as a source, while all other dislocations are targets. The maximum stress change amongst the 1 km × 1 km dislocations is taken as the most likely point where a rupture can propagate between subsections.

This process creates a matrix of stress communications within the fault model. We are primarily interested in links between adjacent subsections; for example, is a rupture more or less likely to move along a given pathway when there are many branching choices? Adjacency between subsections is a three-dimensional problem because dipping and curving faults may be closer at depth than they are on the surface. Therefore, stress change calculations are made between all nearby (<5 km) rupture sections, and each possible rupture branching is considered. Rupture direction matters because stress changes are not necessarily symmetrical between dislocations of different strike, dip, and/or rake. Thus a rupture might need to be assessed from two directions.

Once the list of stress links is gathered, we take two approaches to finding a linking-stress value for use in ranking ruptures. In the first method, we normalize by dividing the sum of the stress changes by the number of links. Each rupture then can be characterized by a single value that describes its continuity and rake consistency. Ruptures with long gaps and/or poorly aligned faults have a smaller mean linking stress than a more continuous version. A second, alternative approach that we pursue is calculation of the "weakest link" within a potential rupture. In this approach, each rupture is ranked by the most difficult bend, gap, or branching within it as indentified by the smallest linking stress between adjacent subsections of the rupture.

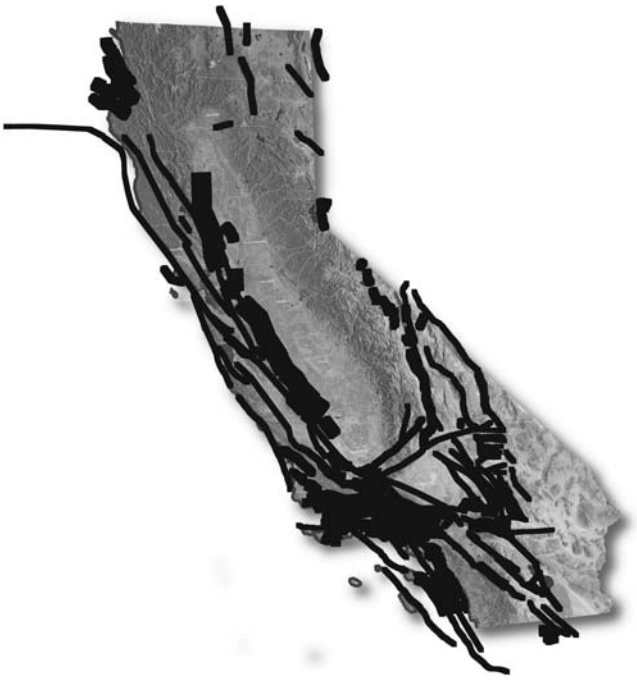

Figure 2. California mapped faults simplified into subsections.

Applications, Caveats, and Sources of Uncertainty

How should the linking stress be used? Can all ruptures be compared directly? For example, a long rupture with 100 subsection links might include just one long gap that produces one unfavorable stress change. Its signal is muted when averaged with the other 99 links, making comparison of this rupture with another in a completely different region or fault system problematic. However, comparison of this value with that from ruptures on the same fault, but that stop short of the gap, could provide useful ranking information. Additionally, ruptures such as this example with one weak link can be directly compared on the basis of the minimum stress change between adjacent sections, which is independent of rupture length.

As discussed above, Coulomb stress change calculations are very sensitive to the distance between source and target dislocations. Therefore, uncertainty related to mapped fault end points has important impact on the magnitude of calculated stress change. This uncertainty can be magnified as the dislocations are projected downdip, which of course is also affected by dip uncertainty. Expert geological assessments can provide informed weighting in settings where a fault end point might, for example, be mapped because of thin sedimentary cover, but the fault actually is thought to persist closer to or even connect directly with another. By comparison, another end point might be very well characterized in hard rock, leaving little doubt. The relative value of these observations would not be accommodated in a stress change calculation unless some quantified uncertainty were given. A further issue arises within some bending, dipping faults because extension of rectangular dislocations downdip can cause overlapping at depth.

Dynamic rupture simulations indicate important effects of preexisting stress distribution (Harris and Day, 1993, 1999) that can determine whether a rupture jumps onto a branching fault or clears a stepover. Additionally, the distribution of slip within a rupture can affect whether a jump occurs or not (Oglesby, 2008; Elliott *et al.*, 2009). These important effects are not addressable with a static stress approach. A feature that is captured in moment-balanced models (Field *et al.*, 2009; Field and Page, 2011) is the relative frequency of ruptures jumping onto a lower slip rate fault versus staying on a major fault, because their frequencies are governed by observed long-term slip rates.

Test Case Results

A subset region from the uniform California forecast (UCERF) region was used for feasibility testing that includes just northern California faults (Fig. 3). The subset region has 20,614 possible ruptures, each of which was assessed with linking stress calculations. In this section we present some example results from the calculations. The potential ruptures range in inferred magnitude from M 5.2 to M 8.2, with the majority being large ruptures (Fig. 4). Rupture magnitudes are calculated using empirically derived area relations (Hanks and Bakun, 2008; Ellsworth "B" relation, WGCEP, 2003, Eqn. 4.5), and are adjusted for aseismic slip on creeping faults (Field *et al.*, 2009).

Figure 3. Test region in northern California/San Francisco Bay region. The faults and their subsections that were used in the method testing are shaded gray.

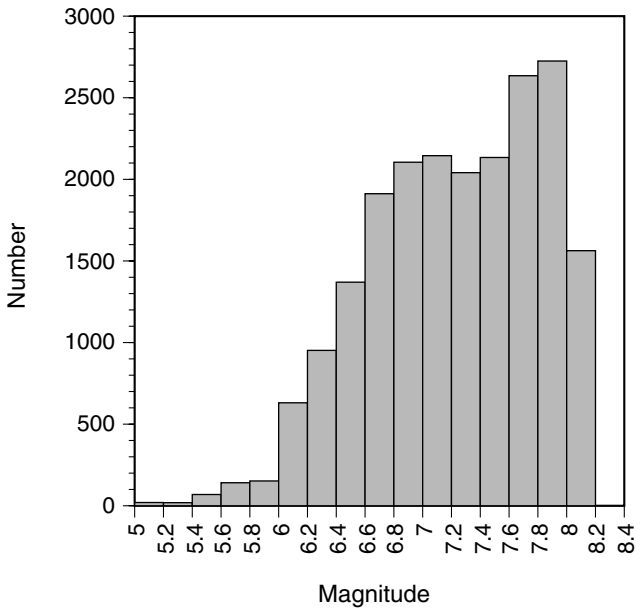

Figure 4. Magnitude distribution of possible ruptures from the test region in northern California/San Francisco Bay region shown in Figure 3. The input distribution is weighted most heavily toward higher magnitudes because many more combinations of a large number of subsections are possible compared with the lower magnitude limit of just two. The output earthquake rate solution is expected to be the inverse because the largest events generate most of the possible moment.

A key issue in earthquake forecasting is establishing the magnitude distribution affecting the region of interest, and

the relative ability of ruptures to jump from fault to fault has an important influence on possible rupture areas. Certainly the magnitude distribution of possible ruptures (Fig. 4) is unlike those observed for large regions, which follow the Gutenberg–Richter power law distribution. Balancing the earthquake rupture model against observed slip rates or plate motion rates reduces the allowable number of the largest (hence most slip) events in the model.

We show examples of linking stress calculations for three possible ruptures in the Hayward–Calaveras fault system in the eastern San Francisco Bay region in Figure 5. The three ruptures have very similar magnitudes, but one involves a step from the Calaveras to the Hayward fault, another lies entirely on the Calaveras, and a third occurs only on the Hayward fault. Relatively small magnitude (M 6.4) ruptures are used for this comparison to minimize complications from other structural influences, such as bends. As would be expected, we find that the continuous rupture on the Calaveras fault has a higher mean linking stress than the jumping rupture by almost double, and a comparison of their weakest links gives the continuous rupture a >6-fold advantage over the branching rupture (Fig. 5). An equivalent magnitude Hayward-fault-only rupture is favored by a factor of $\sim$1.2 over the jumping rupture based on mean linking stress, and by a >5-fold factor based on weakest links.

This example illustrates a method for quantifying the likelihood that a rupture will branch onto an adjacent fault versus remaining on a continuous fault. The stress values could be used as a relative ranking, or could be used to give proportional weight to different rupture scenarios. However, some normalization may be necessary before direct weighting can be employed; the example given in Figure 5 highlights a physical issue with stress-based models. The Calaveras fault has a releasing bend, and thus rupture propagation is calculated to be more favored on it than the slightly restraining orientation of the south Hayward fault. The effect has the Calaveras ruptures favored by a factor of $\sim$1.4 over equivalent Hayward fault events. It is unclear whether a long-term earthquake rupture model would want to give higher weighting to continuous Calaveras fault ruptures over continuous south Hayward ruptures, or whether the method is best applied only at junctions and other geometric features with potential to arrest earthquakes.

We give another example result taken from a circumstance where manual rupture prioritization would be very difficult: a series of imbricate thrust faults in the Mendocino region of northern California (Fig. 6). The mean linking stresses for individual ruptures and the weakest-link stresses are given as proposed ways to rank their relative viability. In this example, a simple continuous rupture that occurs on a single fault trace is compared with more complex, multifault ruptures. Surprisingly, most of the multifault ruptures are higher ranked than the continuous example (Fig. 6). This illustrates that details in fault geometry might favor unexpected ruptures (something that mirrors observations). Other

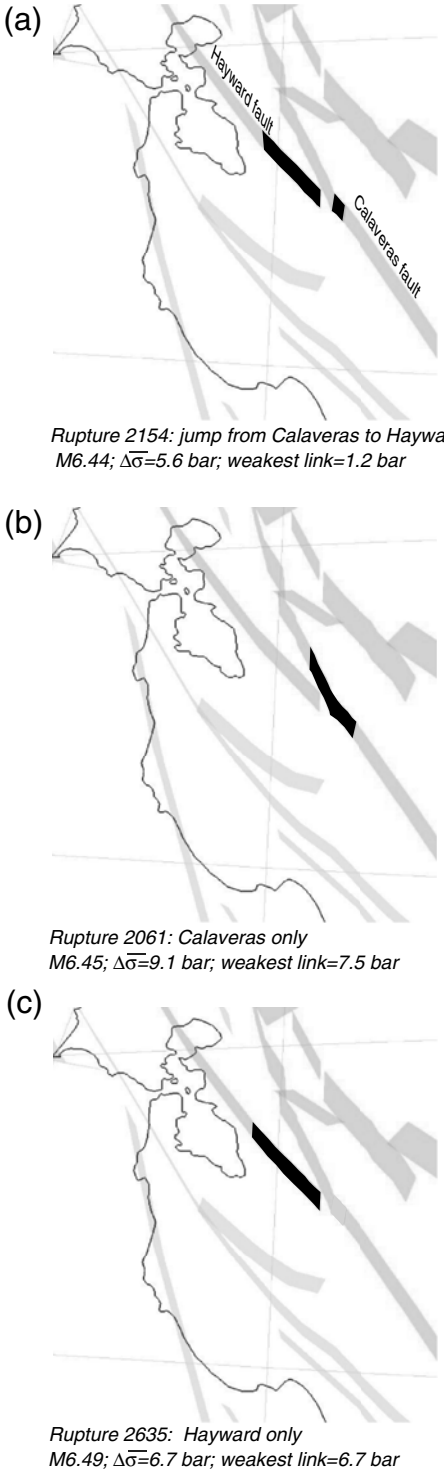

Figure 5. Example rupture ranking using linking stress in the San Francisco Bay region. (a) An M 6.44 model rupture jumps from the Calaveras fault across a gap onto the south Hayward fault; the mean calculated linking stress for this rupture is 5.6 bars. (b) An equivalent magnitude (M 6.45) rupture that is continuous on the Calaveras fault is shown, which has a mean linking stress of 9.1 bars, almost double. (c) The equivalent rupture is contained on the south Hayward fault, which has a mean linking stress of 6.7 bars. Differences between weakest links are more pronounced, with a range from 1.2 bars in the jumping rupture to 7.5 bars for the continuous Calaveras earthquake.

possible ruptures with significant overlap are ranked lower, as might be expected.

We lastly note a few observations from examining all the 20,614 possible rupture ranks as a function of magnitude. The very highest ranked ruptures tend to be among the lowest magnitude considered ($M \sim 6.5$; Fig. 7), though low magnitude ruptures are comparatively rare within the distribution of possible events (Fig. 4). The Appendix lists some of the highest ranked ruptures and their magnitudes (Table A1). Within the top 5000 ranked ruptures, there is a systematic decline in ranking with increasing magnitude. Rank dependence on magnitude is less clear among the lower ranked ruptures (rank < 5000; Fig. 7).

We examine linking stress results in the context of an earthquake-rate solution made for all possible ruptures using the method of Field and Page (2011) within the northern California test region shown in Figure 3. The Field and Page (2011) method is a simulated annealing inversion for earthquake rupture rates that is fit to long-term slip rates, paleoseismic observations, and, optionally, to different magnitude–frequency relations. The method does not depend on fault segmentation, nor any characteristic rupture assumptions, but can encompass these ideas. Of the 20,614 possible ruptures (Fig. 4), 765 are given rates. This result is one of many possible earthquake rate solutions that can be fit to observations. The goal of the linking stress method introduced in this paper is to provide information that might prevent ruptures with low viability being given high rates.

The example earthquake rate solution does include many low-ranked ruptures as identified by calculated linking stresses (Fig. 8a). This outcome is of course an acknowledged possibility with an inversion approach that can include

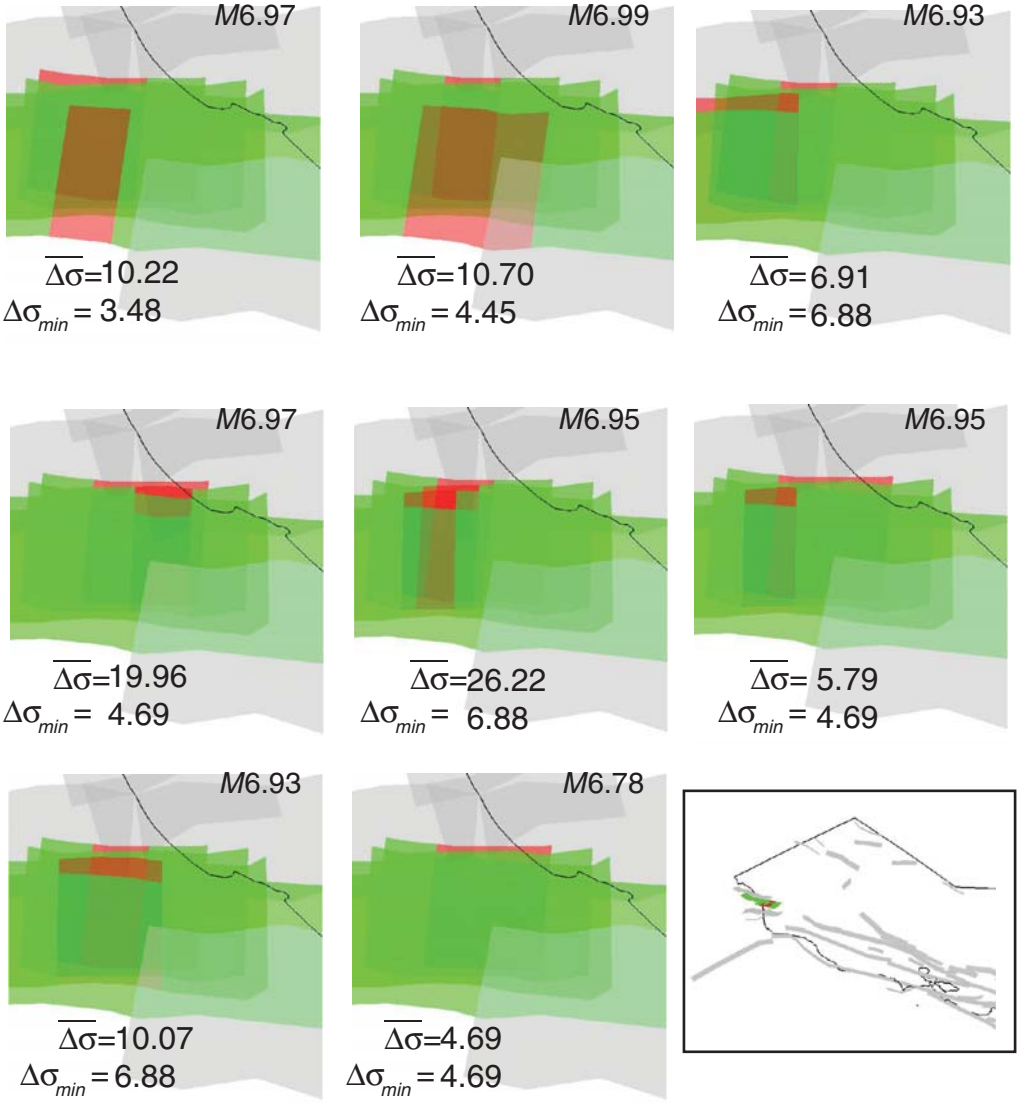

Figure 6. A series of possible ruptures within an imbricate thrust fault system in the Mendocino region of northern California (location shown in inset map). The ruptures (shown in red) can be ranked by comparing the average linking stress calculated for each rupture or the minimum linking stresses. The ruptures with closer connections tend to have higher minimum stresses and thus might be considered more viable.

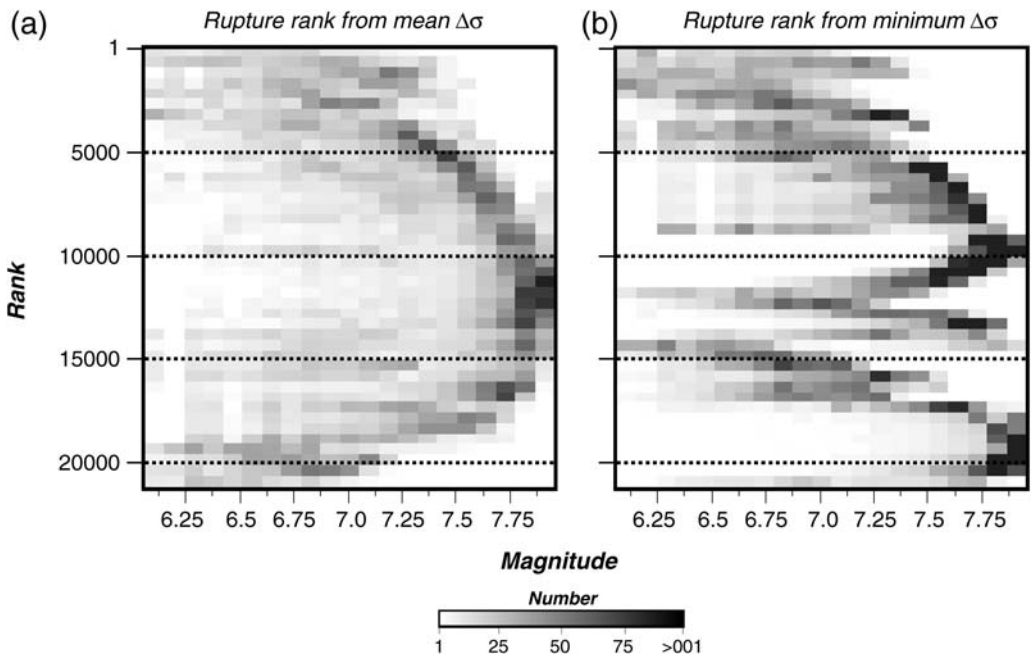

Figure 7. The distribution of possible ruptures as a function of their linking stress rank and magnitude. Top ranking is 1, and lowest is 20,614. Despite the predominance of high magnitude ruptures studied (Fig. 4), we find that most of the very highest ranked ruptures are $M < 7.0$. (a) Ranking is by average linking stress for whole ruptures, and (b) Ranking is performed by the minimum linking stress (weakest link). Generally, the mean stress ranking penalizes larger ruptures slightly more than the weakest link approach because of the potential cumulative effect of multiple inhibiting steps or bends.

all possible ruptures. Thus a quantitative rupture ranking based on expert geologic conclusions, static linking stresses (this study), dynamic rupture simulations, or some combination of all will be necessary to prevent outcomes such as the examples given in Figure 8, where high rates are assigned to unlikely ruptures that have geometric complexity and/or long gaps.

Summary and Conclusions

Linking stress calculations may be useful as a means of ranking ruptures, particularly within fault zones and at points of geometric complexity such as fault steps or bends. We see consistent results in terms of ranking continuous ruptures versus stepping junctions. However, we find also that a change in strike or involvement with nearby subsections does not necessarily imply a lower rank. Calculations are sensitive to details in fault subsection location, especially with respect to how the ends are defined.

We acknowledge that the method proposed here is not a complete representation of the earthquake process. Clearly the pre-stress state, rupture propagation velocity, and dynamic slip distribution all have important roles in determining the viability of a given rupture (Kame *et al.*, 2003; Bhat *et al.*, 2004; Oglesby, 2008; Templeton *et al.*, 2009, 2010). Generally, however, these aspects are not currently considered in probabilistic forecasts, which seek to identify long-term spatial hazard resulting from all possible ruptures. The all-California UCERF methodology generates more than 1 million possible $M > 5$ ruptures; our proposed method is intended as one option for editing out the least likely of these and that employs some simple physics. The alternatives of visual inspection of each possibility or multiple, fully dynamic simulations of each rupture are not currently possible.

We identify two ways to rank ruptures using linking stress: (1) the mean of all linking stresses within a potential rupture, and (2) the minimum linking stress (weakest link) amongst all adjacent subsections. The weakest-link approach is most familiar in terms of how faults are usually segmented from geologic information, and offers a way to avoid issues related to static stress change calculations such as favoring releasing bends along continuous ruptures. This approach may also be the most useful in terms of integrating linking stress calculations with other rupture weighting procedures such as expert geologic interpretation.

Data and Resources

The Working Group on California Earthquake Probabilities maintains the California Reference Geologic Fault Parameter Database at http://wgcep.org/data-ref_fault_db (last accessed November 2011). The fault data are primary input sources for the Uniform California Earthquake Rupture Forecast (UCERF) and are also part of the USGS Quaternary Fault and Fold Database, which can be found at http://earthquake.usgs.gov/hazards/qfaults/ (last accessed November 2011).

Acknowledgments

We very much appreciate reviews by Associate Editor David Oglesby and two anonymous reviewers. Yehuda Ben-Zion and Greg Beroza also

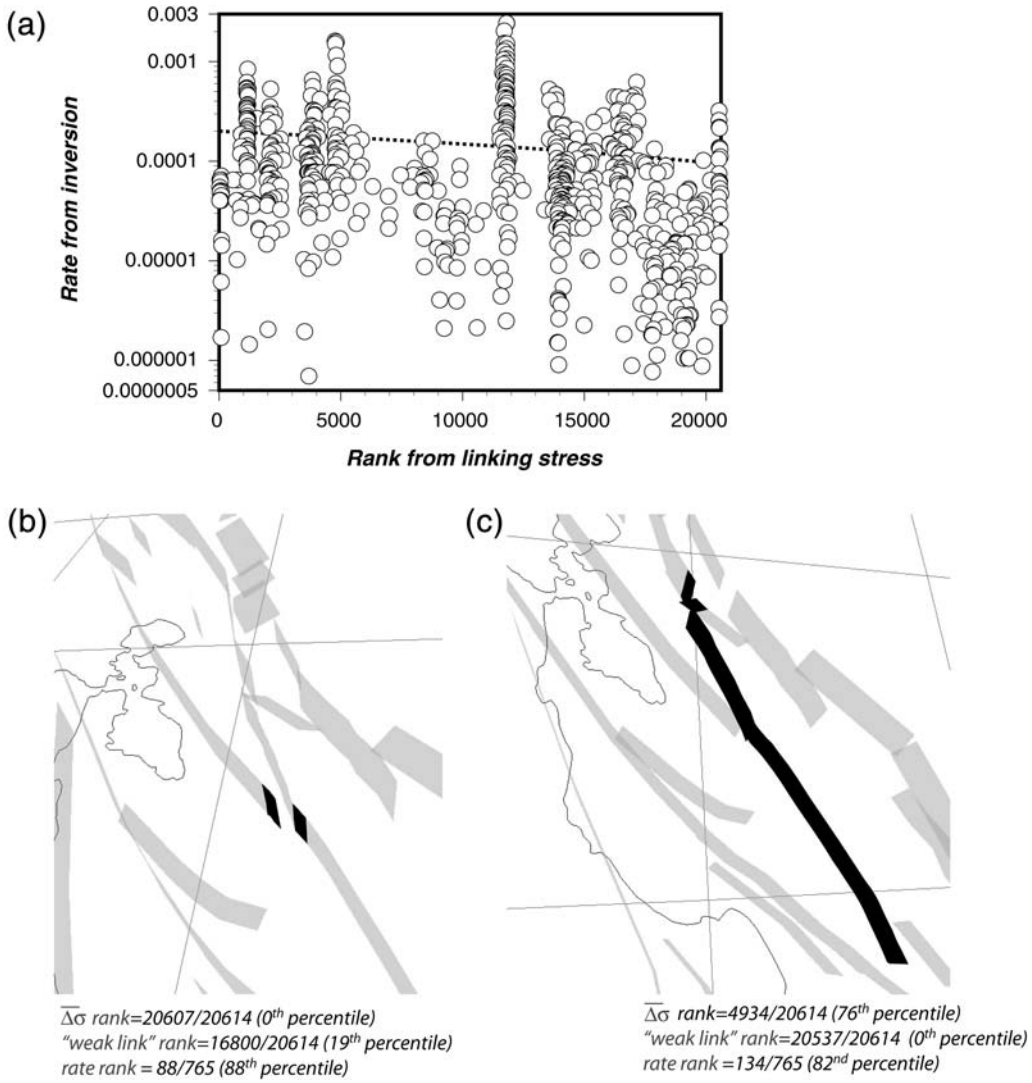

Figure 8. (a) Rupture ranking from linking stress calculations is compared with the annual rupture rate calculated for them using the method of Field and Page (2011). Many low-ranked ruptures are given rates, implying that some discrimination factor may be necessary. Dashed black line gives the best fit to a linear relation between rate and rank, which has a slightly negative slope. (b) and (c) Two example ruptures that are given high rates by the inversion but low ranking from linking stresses are shown. High rates (~80th percentiles) are associated with ruptures that have either complex junctions or long gaps, causing them to have very low percentile (0th) linking-stress ranks.

reviewed a draft as part of the Uniform California Earthquake Rupture Forecast (UCERF) review process.

References

Barka, A. A., and K. Kandinsky-Cade (1988). Strike-slip fault geometry in Turkey and its influence on earthquake activity, *Tectonics* **7,** 663–684.

Bhat, H. S., R. Dmowska, J. R. Rice, and N. Kame (2004). Dynamic slip transfer from the Denali to totschunda faults, Alaska: Testing theory for fault branching, *Bull. Seismol. Soc. Am.* **94,** S202–S213.

Biasi, G., T. Parsons, R. J. Weldon II, and T. E. Dawson (2012). Appendix J, fault-to-fault rupture probabilities, *U.S. Geol. Surv. Open-File Rept.* (in press).

Earthquake Research Committee (2005). *Comprehensive study of probabilisitic seismic hazard map for Japan*, Headquarters for Earthquake Research Promotion, Tokyo, Japan, 125 pp.

Eberhart-Phillips, D., P. J. Haeussler, J. T. Freymueller, A. D. Frankel, C. M. Rubin, P. Craw, N. A. Ratchkovski, G. Anderson, G. A. Carver, A. J. Crone, T. E. Dawson, H. Fletcher, R. Hansen, E. L. Harp, R. A. Harris, D. P. Hill, S. Hreinsdóttir, R. W. Jibson, L. M. Jones, R. Kayen, D. K. Keefer, C. F. Larsen, S. C. Moran, S. F. Personius, G. Plafker, B. Sherrod, K. Sieh, N. Sitar, and W. K. Wallace (2003). The 2002 Denali fault earthquake, Alaska: A large magnitude, slip-partitioned event, *Science* **300,** 1113–1118, doi: 10.1126/science.1082703

Elliott, A. J., J. F. Dolan, and D. D. Oglesby (2009). Evidence from coseismic slip gradients for dynamic control on rupture propagation and arrest through stepovers, *J. Geophys. Res.* **114,** no. B02312, doi: 10.1029/2008JB005969.

Field, E. H., and M. T. Page (2011). Estimating earthquake-rupture rates on a fault or fault system, *Bull. Seismol. Soc. Am.* **101,** 79–92, doi: 10.1785/0120100004.

Field, E. H., T. E. Dawson, K. R. Felzer, A. D. Frankel, V. Gupta, T. H. Jordan, T. Parsons, M. D. Petersen, R. S. Stein, R. J. Weldon II, and C. J. Wills (2009). The Uniform California Earthquake Rupture Forecast, version 2 (UCERF 2), *Bull. Seismol. Soc. Am.* **99,** 2053–2107, doi: 10.1785/0120080049.

Frankel, A. D., M. D. Petersen, C. S. Mueller, K. M. Haller, R. L. Wheeler, E. V. Leyendecker, R. L. Wesson, S. C. Harmsen, C. H. Cramer,

D. M. Perkins, and K. S. Rukstales (2002). Documentation for the 2002 Update of the National Seismic Hazard Maps, *U.S. Geol. Surv. Open-File Rept. OFR-02-420*, 33 pp.

Hanks, T. C., and W. H. Bakun (2008). *M*-log A observations for recent large earthquakes, *Bull. Seismol. Soc. Am.* **98,** 490–494.

Harris, R. A. (1992). Dynamic interaction of parallel strike-slip fault-segments: Some implications for the eastern San Francisco Bay area, in *Proc. of the Second Conference on Earthquake Hazards in the Eastern San Francisco Bay Area*, G. Borchardt, S. E. Hirschfeld, J. J. Lienkaemper, P. McClellan, and I. G. Wong (Editors), Calif. Div. Mines Geol. Spec. Publ., Vol. **113**, 73–80.

Harris, R. A., and S. M. Day (1993). Dynamics of fault interaction: Parallel strike-slip faults, *J. Geophys. Res.* **98,** 4461–4472.

Harris, R. A., and S. M. Day (1999). Dynamic 3D simulations of earthquakes on en echelon faults, *Geophys. Res. Lett.* **26,** 2089–2092.

Kame, N., J. R. Rice, and R. Dmowska (2003). Effects of prestress state and rupture velocity on dynamic fault branching, *J. Geophys. Res.* **108,** 2265, doi: 10.1029/2002JB002189.

Kase, Y., and K. Kuge (1998). Numerical simulation of spontaneous rupture processes on two non-coplanar faults: the effect of geometry on fault interaction, *Geophys. J. Int.* **135,** 911–922.

Klinger, Y. (2010). Relation between continental strike-slip earthquake segmentation and thickness of the crust, *J. Geophys. Res.* **115,** no. B07306, doi: 10.1029/2009JB006550.

Klinger, Y., M. Etchebes, P. Tapponnier, and C. Narteau (2011). Characteristic slip for five great earthquakes along the Fuyun fault in China, *Nat. Geosci.* **4,** 389–392.

Lettis, W., J. Bachhuber, R. Witter, C. Brankman, C. E. Randolph, A. Barka, W. D. Page, and A. Kaya (2002). Influence of releasing step-overs on surface fault rupture and fault segmentation: Examples from the 17 August 1999 Izmit earthquake on the North Anatolian fault, Turkey, *Bull. Seismol. Soc. Am.* **92,** 19–42.

Li, H.-B., Z.-X. Wang, X.-F. Fu, L.-W. Hou, J.-L. Si, Z.-L. Qiu, N. Li, and F.-Y. Wu (2008). The surface rupture zone distribution of the Wenchuan earthquake (M_S 8, 0) happened on May 12th, 2008, *Geol. China* **35,** 803–813.

Liu-Zeng, J., Y. Klinger, X. Xu, C. Lasserre, G. Chen, W. Chen, P. Tapponnier, and B. Zhang (2007). Millennial recurrence of large earthquakes on the Haiyuan fault near Songshan, Gansu Province, China, *Bull. Seismol. Soc. Am.* **97,** 14–34.

Lozos, J. C., D. D. Oglesby, B. Duan, and S. G. Wesnousky (2011). The effects of double fault bends on rupture propagation: A geometrical parameter study, *Bull. Seismol. Soc. Am.* **101,** 385–398, doi: 10.1785/0120100029.

McCann, W. R., S. P. Nishenko, L. R. Sykes, and J. Krause (1979). Seismic gaps and plate tectonics: Seismic potential for major boundaries, *Pure Appl. Geophys.* **117,** 1082–1147.

National Seismic Hazard Maps for Japan (2005). *Headquarters for Earthquake Research Promotion*, 162 pp.

Oglesby, D. (2008). Rupture termination and jump on parallel offset faults, *Bull. Seismol. Soc. Am.* **98,** 440–447, doi: 10.1785/0120070163.

Okada, Y. (1992). Internal deformation due to shear and tensile faults in a half-space, *Bull. Seismol. Soc. Am.* **82,** 1018–1040.

Petersen, M. D., A. D. Frankel, S. C. Harmsen, C. S. Mueller, K. M. Haller, R. L. Wheeler, R. L. Wesson, Y. Zeng, O. S. Boyd, D. M. Perkins, N. Luco, E. H. Field, C. J. Wills, and K. S. Rukstales (2008). Documentation for the 2008 update of the United States National Seismic Hazard Maps, *U.S. Geol. Surv. Open-File Rept. 2001-1128*, 61 pp.

Romeo, R. W. (2005). Earthquake hazard in Italy, 2001–2030, *Nat. Hazards* **36,** 383–405, doi: 10.1007/s11069-005-1939-1.

Scholz, C. H., R. Ando, and B. E. Shaw (2010). The mechanics of first order splay faulting: The strike-slip case, *J. Struct. Geol.* **32,** 118–126.

Schwartz, D. P., and K. J. Coppersmith (1984). Fault behavior and characteristic earthquakes: examples from the Wasatch and San Andreas fault zones, *J. Geophys. Res.* **89,** 5681–5698.

Simpson, R. W., and P. A. Reasenberg (1994). Earthquake-induced static-stress changes on central California faults, *U.S. Geol. Surv. Prof. Pap. 1550-F*, 55–89.

Templeton, E. L., A. Baudet, H. S. Bhat, R. Dmowska, J. R. Rice, A. J. Rosakis, and C.-E. Rousseau (2009). Finite element simulations of dynamic shear rupture experiments and dynamic path selection along kinked and branched faults, *J. Geophys. Res.* **114,** no. B08304, doi: 10.1029/2008JB006174.

Templeton, E. L., H. S. Bhat, R. Dmowska, and J. R. Rice (2010). Dynamic rupture through a branched fault configuration at Yucca Mountain, and resulting ground motions, *Bull. Seismol. Soc. Am.* **100,** 1485–1497.

Wechsler, N., Y. Ben-Zion, and S. Christofferson (2010). Evolving geometrical heterogeneities of fault trace data, *Geophys. J. Int.* **182,** 551–567.

Wesnousky, S. G. (1994). The Gutenberg–Richter or Characteristic Earthquake Distribution, Which Is It?, *Bull. Seismol. Soc. Am.* **84,** 1940–1959.

Wesnousky, S. G. (2006). Predicting the endpoints of earthquake ruptures, *Nature* **444,** 358–360.

Wesnousky, S. G. (2008). Displacement and geometrical characteristics of earthquake surface ruptures: Issues and implications for seismic-hazard analysis and the process of earthquake rupture, *Bull. Seismol. Soc. Am.* **98,** 1609–1632, doi: 10.1785/0120070111.

Wesnousky, S. G., and G. P. Biasi (2011). The length to which an earthquake will go to rupture, *Bull. Seismol. Soc. Am.* **101,** 1948–1950.

Working Group on California Earthquake Probabilities (1988). Probabilities of large earthquakes occurring in California on the San Andreas fault, *U.S. Geol. Surv. Open-File Rept. 88-398*, 62 pp.

Working Group on California Earthquake Probabilities (1990). Probabilities of large earthquakes in the San Francisco Bay region, California, *U.S. Geol. Surv. Circ.* **1053,**, 51 pp.

Working Group on California Earthquake Probabilities (WGCEP) (1995). Seismic hazards in Southern California: Probable earthquakes, 1994 to 2024, *Bull. Seismol. Soc. Am.* **85,** 379–439.

Working Group on California Earthquake Probabilities (WGCEP) (2003). Earthquake probabilities in the San Francisco Bay region: 2002 to 2031, *U.S. Geol. Surv. Open-File Rept. 03-214*, 235 pp.

Zielke, O., R. Arrowsmith, L. G. Ludwig, and S. O. Akçiz (2010). Slip in the 1857 and earlier large earthquakes along the Carrizo Plain, San Andreas Fault, *Science* **327,** 1119–1122.

Appendix

We provide a table (Table A1) of the 100 highest ranked earthquake ruptures from the northern California test region (Fig. 3) as found through linking stress calculations. All the top-ranked ruptures are less than *M* 7 because the odds of shorter ruptures including inhibiting steps or bends are lower.

Table A1

A List of the Top 100 Ranked Ruptures with Ranks Given for Mean Linking Stress and Weakest Links

M	Number Subs	Mean $\Delta\sigma$	Min.$\Delta\sigma$	Rank (Mean $\Delta\sigma$)	Rank (Min.$\Delta\sigma$)
6.1	2	48.76	48.76	1	1
6.1	2	45.55	45.55	2	2
6.1	2	41.75	41.75	3	3
6.1	2	39.17	39.17	4	4
6.1	2	39.09	39.09	5	5
6.1	2	35.23	35.23	6	6
6.1	2	29.71	29.71	10	7
6.1	2	29.59	29.59	12	8
6.1	2	28.74	28.74	14	9
6.1	2	27.17	27.17	15	10

(*continued*)

Table A1 (*Continued*)

M	Number Subs	Mean $\Delta\sigma$	Min.$\Delta\sigma$	Rank (Mean $\Delta\sigma$)	Rank (Min.$\Delta\sigma$)
6.3	3	33.03	26.88	7	11
6.1	2	26.88	26.88	17	12
6.1	2	24.86	24.86	22	13
6.1	2	24.06	24.06	29	14
6.1	2	24.06	24.06	31	15
6.1	2	20.88	20.88	39	16
6.1	2	20.71	20.71	40	17
6.1	2	19.14	19.14	58	18
6.1	2	18.97	18.97	61	19
6.3	3	19.44	18.16	56	20
6.1	2	18.16	18.16	67	21
6.1	2	16.95	16.95	83	22
6.1	2	16.24	16.24	95	23
6.1	2	15.41	15.41	117	24
6.1	2	15.24	15.24	122	25
6.1	2	15.21	15.21	123	26
6.1	2	14.22	14.22	172	27
6.1	2	14.17	14.17	179	28
6.1	2	14.14	14.14	183	29
6.1	2	14.11	14.11	185	30
6.1	2	14.08	14.08	187	31
6.1	2	14.01	14.01	201	32
6.3	3	14.04	13.99	194	33
6.1	2	13.99	13.99	214	34
6.3	3	14.06	13.94	190	35
6.1	2	13.94	13.94	227	36
6.4	4	14.00	13.92	210	37
6.3	3	13.96	13.92	226	38
6.1	2	13.92	13.92	230	39
6.5	5	14.02	13.90	196	40
6.6	6	14.02	13.90	199	41
6.4	4	14.00	13.90	206	42
6.7	7	14.00	13.90	208	43
6.3	3	13.99	13.90	212	44
6.4	4	13.99	13.90	213	45
6.5	5	13.98	13.90	220	46
6.4	4	13.97	13.90	222	47
6.5	5	13.97	13.90	223	48
6.6	6	13.97	13.90	224	49
6.3	3	13.92	13.90	229	50
6.1	2	13.90	13.90	231	51
6.1	2	13.87	13.87	235	52
6.4	4	14.05	13.85	191	53
6.5	5	14.03	13.85	195	54
6.7	7	14.01	13.85	200	55
6.7	8	14.01	13.85	202	56
6.3	3	14.01	13.85	203	57
6.6	6	14.00	13.85	207	58
6.8	9	14.00	13.85	209	59
6.3	3	14.00	13.85	211	60
6.7	7	13.99	13.85	215	61
6.6	6	13.99	13.85	216	62
6.4	4	13.99	13.85	217	63
6.7	8	13.98	13.85	218	64
6.5	5	13.97	13.85	225	65
6.1	2	13.85	13.85	241	66
6.1	2	13.85	13.85	242	67
6.3	3	13.85	13.83	239	68
6.4	4	13.85	13.83	240	69
6.3	3	13.84	13.83	248	70
6.1	2	13.83	13.83	254	71
6.3	3	14.02	13.82	197	72
6.3	3	13.85	13.82	245	73
6.5	5	13.84	13.82	246	74
6.4	4	13.84	13.82	247	75
6.1	2	13.82	13.82	258	76
6.1	2	13.82	13.82	259	77
6.6	6	13.84	13.81	249	78
6.4	4	13.83	13.81	250	79
6.5	5	13.83	13.81	252	80
6.3	3	13.82	13.81	260	81
6.1	2	13.81	13.81	262	82
6.7	7	13.83	13.80	253	83
6.6	6	13.83	13.80	255	84
6.5	5	13.83	13.80	256	85
6.4	4	13.81	13.80	261	86
6.3	3	13.81	13.80	263	87
6.1	2	13.80	13.80	265	88
6.1	2	13.66	13.66	286	89
6.3	3	29.40	13.25	13	90
6.1	2	13.25	13.25	365	91
6.3	3	13.64	13.16	291	92
6.1	2	13.16	13.16	381	93
6.3	3	13.52	13.02	320	94
6.1	2	13.02	13.02	422	95
6.1	2	12.52	12.52	555	96
6.1	2	12.35	12.35	610	97
6.1	2	12.32	12.32	621	98
6.1	2	12.26	12.26	652	99
6.3	3	12.30	12.25	633	100

(*continued*)

This behavior could be a factor in the commonly observed Gutenberg–Richter magnitude frequency distribution in large regions.

U.S. Geological Survey
345 Middlefield Rd.
Menlo Park, California 94025
(T.P.)

U.S. Geological Survey
Denver Federal Center
PO Box 25046 MS-966
Denver, Colorado 80225
(E.H.F.)

U.S. Geological Survey
525 South Wilson Ave.
Pasadena, California 91106-3212
(M.T.P.)

Southern California Earthquake Center
University of Southern California
3651 Trousdale Parkway, Suite 169
Los Angeles, California 90089-0742
(K.M.)

Manuscript received 22 December 2011